ACS APPLIED MATERIALS & INTERFACES

Research Article

www.acsami.org

Direct Transformation from Graphitic C_3N_4 to Nitrogen-Doped Graphene: An Efficient Metal-Free Electrocatalyst for Oxygen Reduction Reaction

Jiajie Li,[†] Yumin Zhang,[†] Xinghong Zhang,[†] Jiecai Han,[†] Yi Wang,[‡] Lin Gu,[*,§] Zhihua Zhang,[⊥] Xianjie Wang,[∥] Jikang Jian,[⊗] Ping Xu,[*,▽] and Bo Song[*,†,‡,▽]

[†]Centre for Composite Materials, Harbin Institute of Technology, Harbin 150080, People's Republic of China

[‡]Academy of Fundamental and Interdisciplinary Sciences, Harbin Institute of Technology, Harbin 150080, People's Republic of China

[§]Beijing National Laboratory for Condensed Matter Physics, Institute of Physics, Chinese Academy of Sciences, Beijing 100190, People's Republic of China

[⊥]Liaoning Key Materials Laboratory for Railway, School of Materials Science and Engineering, Dalian Jiaotong University, Dalian 116028, People's Republic of China

[∥]Department of Physics, Harbin Institute of Technology, Harbin 150080, People's Republic of China

[⊗]School of Physics and Optoelectronic Engineering, Guangdong University of Technology, Guangzhou 510006, People's Republic of China

[▽]Department of Chemistry, Harbin Institute of Technology, Harbin 150080, People's Republic of China

Supporting Information

ABSTRACT: Carbon-based nanomaterials provide an attractive perspective to replace precious Pt-based electrocatalysts for oxygen reduction reaction (ORR) to enhance the practical applications of fuel cells. Herein, we demonstrate a one-pot direct transformation from graphitic-phase C_3N_4 (g-C_3N_4) to nitrogen-doped graphene. g-C_3N_4, containing only C and N elements, acts as a self-sacrificing template to construct the framework of nitrogen-doped graphene. The relative contents of graphitic and pyridinic-N can be well-tuned by the controlled annealing process. The resulting nitrogen-doped graphene materials show excellent electrocatalytic activity toward ORR, and much enhanced durability and tolerance to methanol in contrast to the conventional Pt/C electrocatalyst in alkaline medium. It is determined that a higher content of N does not necessarily lead to enhanced electrocatalytic activity; rather, at a relatively low N content and a high ratio of graphitic-N/pyridinic-N, the nitrogen-doped graphene obtained by annealing at 900 °C (NGA900) provides the most promising activity for ORR. This study may provide further useful insights on the nature of ORR catalysis of carbon-based materials.

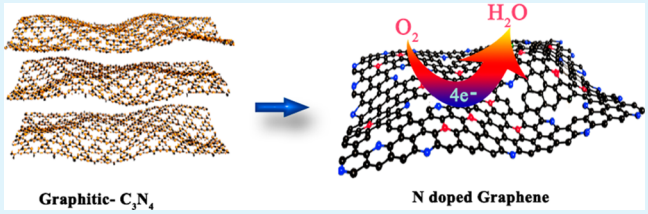

KEYWORDS: *graphitic C_3N_4, N-doped graphene, oxygen reduction, electrocatalysis, metal-free*

1. INTRODUCTION

Efficiency of the oxygen reduction reaction (ORR) at the cathode has become one of the most challenging tasks for various energy devices including fuel cells and metal−air batteries.[1,2] To date, Pt-based materials are still the most widely used catalysts, even though their further application is limited because of their high cost, limited stability, poor tolerance to methanol, and sluggish kinetics.[3−5] Great efforts have been devoted to developing highly active catalysts for ORR with comparable activity to Pt, but with higher durability and lower cost, including Pt-based alloys,[6−8] transition-metal catalysts,[9−11] and carbon-based nanomaterials.[12−20] Notably, carbon-based materials are considered as promising catalysts because of their low cost, environmental friendliness, high electrocatalytic selectivity, and good durability.[21−25]

Doping of heteroatoms such as N into carbon-based materials significantly contributed to the better selectivity for ORR because the N atom with five valence electrons could easily shift the neutrally charged adjacent carbon atoms and create positively charged sites, favoring O_2 adsorption and reduction.[26−30] The catalytic activity of N-doped carbon is affected by the pH value of the electrolytes, four-electron pathway is more favorable in alkaline electrolytes as compared to acidic electroytes.[31,32] In general, N-doped carbon-based materials are prepared mainly by two methods: postdoping[26,27,32−34] and *in situ* direct-doping.[21−23] However, these

Received: May 4, 2015
Accepted: August 20, 2015
Published: August 20, 2015

ACS Publications © 2015 American Chemical Society

DOI: 10.1021/acsami.5b03845
ACS Appl. Mater. Interfaces 2015, 7, 19626−19634

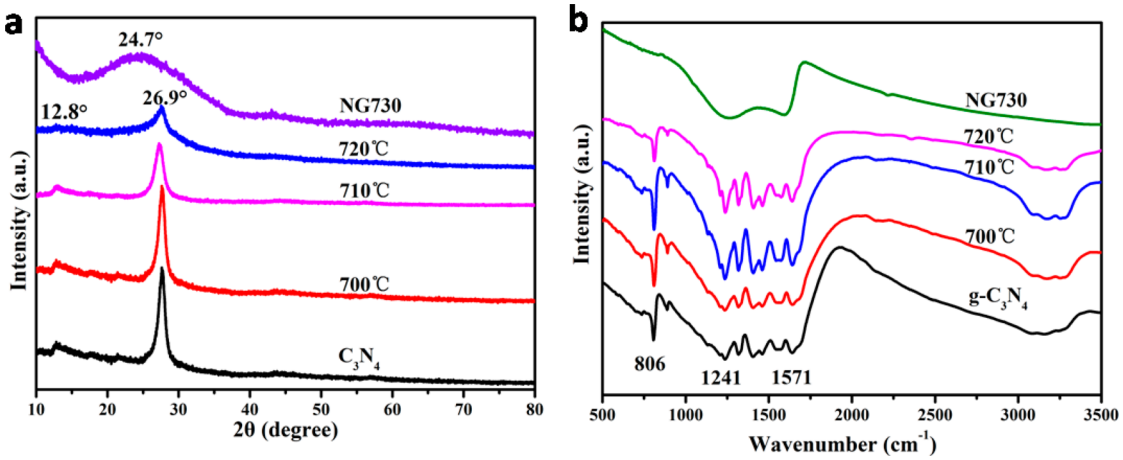

Figure 1. (a) XRD patterns and (b) FT-IR spectra of the samples heated at different temperatures.

pathways have obvious disadvantages including low efficiency, residual metallic impurity, and requirement of multiple organic precursors.[22,32] The postdoping method usually involves a chemical pretreatment with HNO_3, NH_3, or HCN to introduce the N atom, which may lead to a poor control over the chemical homogeneity, reproducibility, and crystal structure.[32,35] Therefore, it is urgent to develop a green, highly efficient, and environmentally benign route to synthesize N-doped carbon-based materials with high ORR catalytic activity. Notably, even with great effort toward the ORR origin, the nature of catalytic sites has been heavily debated because of the following two technological barriers: (1) N-doping level and type are varied significantly depending on the synthesis conditions; and (2) in most cases, an inevitable operation to remove the template or activate the samples using potassium hydroxide deteriorates the crystallinity of the samples, thwarting the attempts to get an unambiguous understanding of the catalytic nature.[32,36,37] Thus, the development of a synthesis route for metal-free N-doped carbon materials that can both exhibit superior activity toward ORR and reveal the nature of catalytic sites is highly desired. In a recent study, we synthesized graphene/graphene-tube nanocomposites derived from metal−organic frameworks (MOFs) as highly efficient ORR catalysts, particularly for nonaqueous Li−O_2 battery cathodes,[38] but metal impurities were still present.

Metal-free graphitic-phase C_3N_4 (g-C_3N_4), a semiconductor with a band gap of ∼2.64 eV,[39] has received increasing attention owing to its potential application in ORR,[40] photocatalysis,[19,41−44] bioimaging,[45,46] etc. Carbon nitride (like CN*x*, g-C_3N_4) shows reasonably good ORR activity in acidic medium, but its poor electrical conductivity hampers its widespread applications in PEMFCs.[28] In particular, because of its high N content, g-C_3N_4 was often used as the N source to synthesize N-doped materials or incorporate into mesoporous or conductive carbon as the potential candidate for ORR.[47] It is therefore of great interest to explore the possibility of utilizing this novel framework that only contains carbon and nitrogen elements to synthesize N-doped carbon materials. The unique crystal structure with no other metal impurity element makes it an ideal self-sacrificing template to synthesize N-doped graphene-like carbon materials.[47] However, unsuccessful control over the heat treatment process of g-C_3N_4 usually leads to gaseous components ($C_2N_2^+$,$C_3N_2^+$, N_2 etc.) as the final products.[48,49] Herein, we demonstrate, for the first time, a novel one-pot strategy to synthesize N-doped graphene through a direct transformation from bulk g-C_3N_4. The as-prepared N-doped graphene exhibited excellent catalytic activity for ORR, which is comparable to the commercial Pt/C (20 wt %, E-TEK), but with even better stability and lower cost. The direct transformation from g-C_3N_4 to N-doped graphene may provide new insight for the design and synthesis of nonprecious metal catalyst, and help to reveal the ORR catalytic nature of N-doped carbon materials.

2. EXPERIMENTAL SECTION

2.1. Synthesis of N-Doped Graphene. The g-C_3N_4 was synthesized following a procedure described in a previous report.[42] In detail, the as-purchased melamine (99.99%, Alfa Aesar) was heated at 600 °C for 4 h in a conventional tube furnace under a high-purity Ar (99.999%) flow of 50 standard-state cubic centimeters per minute (sccm) with a ramp rate of 2.3 °C/min. Next, 2 g of the as-prepared g-C_3N_4 powder was placed in a quartz tube (20 cm × Φ 1.8 cm) with one terminal open. Then, a quartz plug (5 cm × Φ 1.7 cm) was inserted from the open side. After that, the configured quartz tube was placed in a conventional tube furnace, and the open side was placed at the downstream. The furnace was heated to 730−790 °C for 1 h with a ramp rate of 2 °C/min under a high-purity argon (99.9999%) flow of 100 sccm. The annealing was performed in tube furnace at 800−1000 °C for 2 h at a ramp rate of 5 °C/min under a high-purity N_2 (99.999%) flow of 50 sccm.

2.2. Characterization. SEM images were recorded on a Hitachi SU8020 scanning electron microscope. XRD measurements were performed on a Rigaku D/max 2500 X-ray diffractometer (Cu Kα radiation). TEM images, energy-dispersive EDX spectra, and elemental mapping were collected on a JEM-2100F. X-ray photoelectron spectra were recorded on an ESCALAB MKII using Mg Kα as the excitation source. The ICP measurements were conducted on a PerkinElmer Optima 3300DV inductively coupled plasma (ICP) spectrometer for elemental analysis. Raman spectra were collected on an HR 800 using a 633 nm laser. FT-IR spectra were recorded on a PerkinElmer spectrometer in the range 4000−400 cm^{-1} with a resolution of 4 cm^{-1}. Brunauer−Emmett−Teller (BET) specific surface areas were measured by nitrogen adsorption−desorption analyses using a Micromeritics ASAP 2020.

2.3. Electrochemical Measurements. All the electrochemical measurements were carried out using a CHI 650 D potentiostat in a conventional three-electrode cell using Ag/AgCl (3 M KCl) and a platinum wire as the reference and counter electrodes, respectively. The as-prepared catalysts were dispersed in a mixture of water, ethanol, and Nafion (5%) (volume ratio = 1:1:0.2) to form a 4 mg mL^{-1} suspension. An RDE with a glassy carbon disk (3.0 mm in diameter) served as the substrate of the working electrode for evaluating the ORR activity and selectivity of various catalysts. The

DOI: 10.1021/acsami.5b03845
ACS Appl. Mater. Interfaces 2015, 7, 19626−19634

loading of catalyst is calculated to be about 20 μg on the electrode surface. Before use, the glassy carbon electrodes in RDE were polished using aqueous alumina suspension. For comparison, a 4 mg mL^{-1} Pt/C suspension (20 wt %, E-TEK) was also prepared following the same procedure as described above. Cyclic voltammetry (CV) measurements of different catalysts were performed in an Ar/O_2-saturated KOH (0.1 M) solution in the potential range of 0 and 1.2 V vs RHE at a scan rate of 50 mV s^{-1}. The electrochemical activity was measured in a common flow cell reactor using the RDE technique. In our work, the onset potential of these samples is defined as the potential at the current density of 0.1 mA cm^{-2}.

3. RESULTS AND DISCUSSION

Direct transformation from g-C_3N_4 to N-doped graphene was carried out under Ar atmosphere, as shown in Scheme S1 (the experimental configuration is shown in Figure S1). In a previous study, it is generally accepted that g-C_3N_4 will be decomposed completely to gaseous products above 750 °C, but N-doped graphene can be prepared with the assistance of glucose.[47] However, oxygen-containing groups are inevitably present in the N-doped graphene by using the glucose as the starting material, which hinders the further investigation of the role of N for ORR. Here, we demonstrate that g-C_3N_4 can be directly transformed into N-doped graphene via a modified solid-state reaction (see the Experimental Section for details). Briefly, the precursor of bulk g-C_3N_4 was placed in a one-terminal closed quartz tube coordinated with a quartz plug (see Scheme S1 and Figure S1) in a tube furnace. Under this controlled process, N-doped graphene with a high yield of ~76−78% (calculated based on the carbon obtained from g-C_3N_4) was obtained. X-ray diffraction (XRD) pattern (Figure 1a) of the as-obtained g-C_3N_4 shows the typical diffraction peaks of g-C_3N_4 (The International Centre for Diffraction Data, ICDD-PDF-4+, card no. 01-078-1747, space group *R*3*m*) located at ~12.8° and ~26.9°, corresponding to the lattice planes parallel to the *c*-axis and (002) plane, respectively. With the increase in temperature from 700 to 720 °C (Figure 1a), the diffraction peak at ~12.8° gradually disappeared, and the intensity of the peak at ~26.9° also decreased remarkably. In NG730 (the product synthesized at 730 °C), a broad peak appeared at ~24.7°, indicating a successful transformation from g-C_3N_4 into carbon materials with a low degree of graphitization. This conversion was further confirmed by Raman spectra (Figure S2) and FT-IR spectra (Figure 1b). The characteristic Raman peaks at 705, 746, 975, 1231, and 1310 cm^{-1} of g-C_3N_4 agree well with the previous report.[50] After the controlled heat treatment, typical G band (~1580 cm^{-1}) and D band (~1347 cm^{-1}) of carbon materials were observed, a convincing evidence confirming the successful transformation from g-C_3N_4 to carbon materials at 730 °C.[51,52] In Figure 1b, the FT-IR spectrum of raw g-C_3N_4 have several strong bands in the range of 1200−1650 cm^{-1}, with the peaks at ~1241, 1406, and 1571 cm^{-1} corresponding to the typical stretching modes of CN heterocycles.[53] Additionally, the characteristic breathing mode of triazine units at 806 cm^{-1} was observed.[50,53] Below 730 °C, all samples show the similar FT-IR spectrum compared with g-C_3N_4. After heated at 730 °C, the C═N bonding (~1600 cm^{-1}) and C—N bonding (~1300 cm^{-1}) of nitrogen are clearly formed.[54] In addition, the first-principles calculations also suggest that this transformation is favorable in energy (Figures S3 and S4). Corresponding to the structure transition, SEM (Figure 2a, Figure S5) and TEM images (Figure 2b, Figure S6) exhibited a clear morphological evolution from a dense solid (g-C_3N_4) to loose agglomerates (carbon materials). The ring-like mode in the selected-area electron diffraction (SAED) pattern (inset of Figure 2b) confirms that at this stage the as-prepared carbon materials are amorphous in nature. However, a high-resolution TEM (HRTEM) image (Figure 2c) clearly shows that NG730 is graphene with 4−6 layers. The scanning transmission electron microscopy (STEM) image in Figure 2d displays that N element (inset of Figure 2d) is homogeneously distributed in NG730, and this carbon material is highly doped by N. Brunauer−Emmett−Teller (BET) analysis shows a high surface area of ~750 m^2 g^{-1} for NG730 (Figure S7).

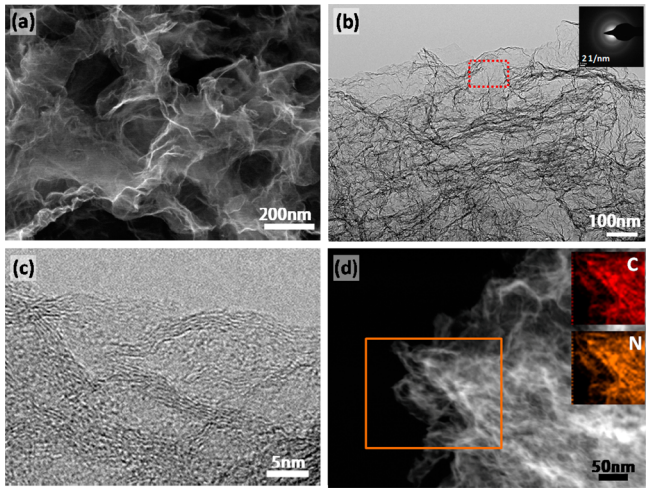

Figure 2. Structural evolution of N-doped graphene by electron microscopy. (a) FE-SEM and (b) TEM images of NG730; the inset of panel b shows the selected-area electron diffraction (SAED) pattern of NG730. (c) HRTEM image of NG730. (d) Scanning TEM image of the NG730 and energy-dispersive X-ray spectrometry elemental maps of C and N (inset in panel d), respectively.

N-Doped carbon materials have been widely studied as efficient ORR electrocatalysts.[21,33] However, cyclic voltammetry (CV) and linear sweep voltammetry (LSV) measurements performed in 0.1 M KOH indicate that the ORR performance of NG730 is very limited (Figure S8), probably owing to the low graphitic degree and incomplete reconstruction of the carbon framework under the current heat treatment conditions. To improve the ORR performance, the as-prepared NG730 was further annealed at higher temperatures (800−1000 °C at an interval of 50 °C, denoted as NGA800, NGA850, etc.) to tune both the graphitization degree and N content. NGA800-NGA1000 showed almost same XRD patterns (Figure 3a). However, the I_D/I_G band intensity ratio in Raman spectra (Figure 3b) decreased from ~1.1 (NG730) to ~0.84 (NGA1000), indicating that the graphitization degree has been significantly improved with increased annealing temperature.[51,55] The annealed samples have similar sheet features (Figure 4a, Figure S9), with loose agglomerates with sizes of several micrometers. AFM imaging of NGA900 (Figure 4b) directly proves the layer structure of the sheets with a layer thickness between 0.39 and 1.02 nm, matching well with the thickness of mono and few-layer graphene, respectively.

The chemical bonding of the samples during the annealing process was evaluated by FT-IR spectroscopy (Figure S10). The NGA samples showed similar spectra to NG730. After annealed, the relative intensity of both C═N bonds (~1592 cm^{-1}) and C—N bonds (~1250 cm^{-1}) gradually decreased,[22] indicating the decreased total N content in NGA samples. To

DOI: 10.1021/acsami.5b03845
ACS Appl. Mater. Interfaces 2015, 7, 19626−19634

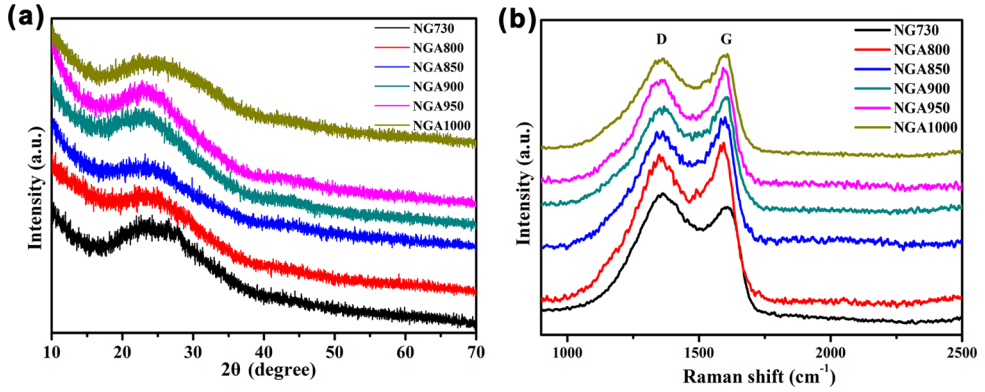

Figure 3. (a) XRD patterns and (b) Raman spectra of NG730 and annealed samples.

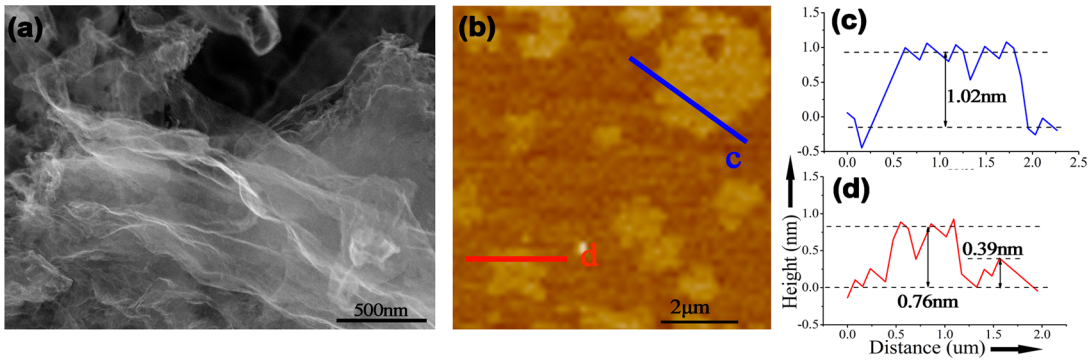

Figure 4. (a) SEM, (b) AFM image of NGA900 and corresponding height measurements (c, d).

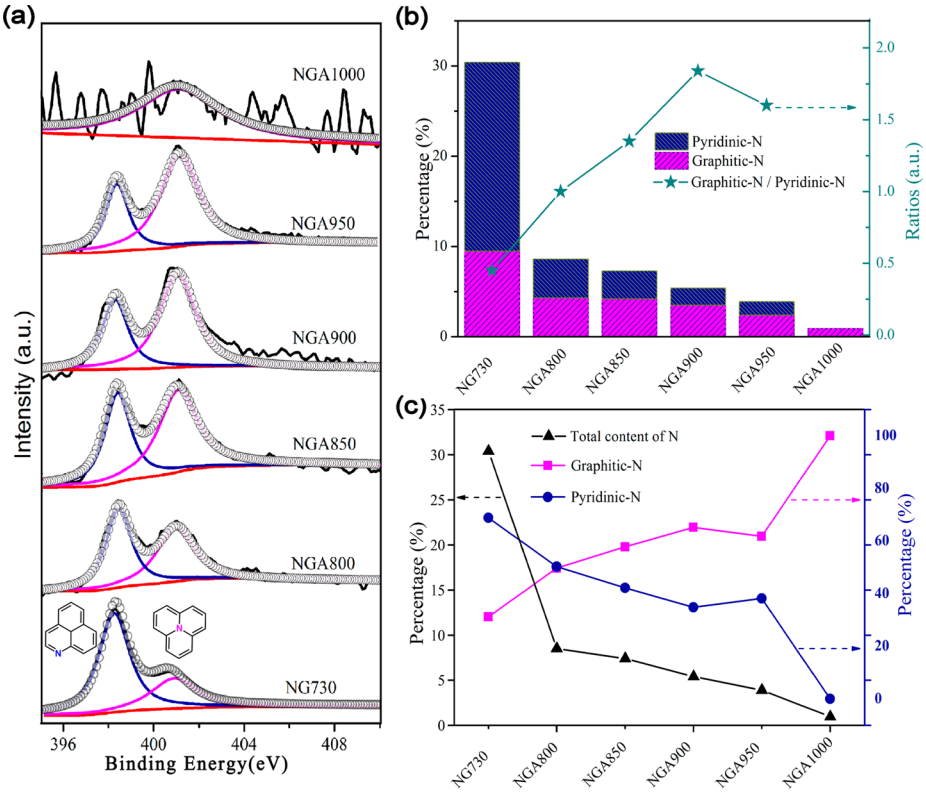

Figure 5. (a) High-resolution N 1s XPS spectra of the as-prepared samples. (b) Content change and ratio of graphitic-N/pyridinic-N of different samples. (c) Graphitic-N, pyridinic-N, and total N contents of different samples.

explore further the N content and species, the chemical structure of the resulting N-doped graphene was elucidated by X-ray photoelectron spectroscopy (XPS) (Figure 5a and Figure S11). As can be seen, the N 1s spectrum could be fitted into

DOI: 10.1021/acsami.5b03845
ACS Appl. Mater. Interfaces 2015, 7, 19626−19634

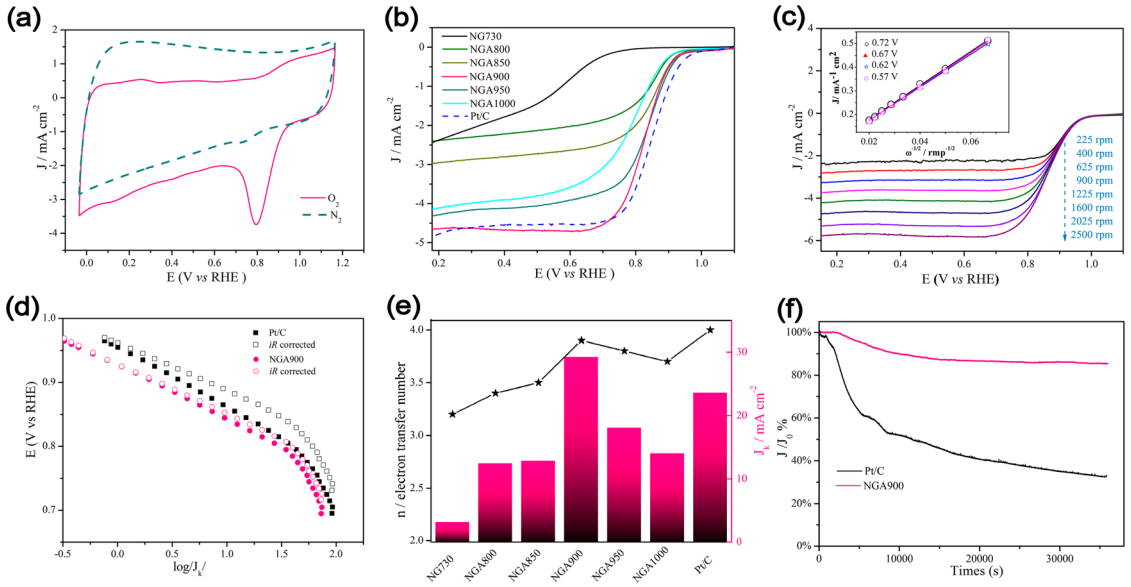

Figure 6. Electrocatalytic performance of the N-doped graphene samples. (a) CV curves of NGA900 in a N_2- or O_2-saturated 0.1 M KOH aqueous solution at a scan rate of 50 mV s^{-1}. (b) Linear scanning voltammograms (LSV) of the as-prepared samples and Pt/C catalyst (20 wt %, E-TEK) at 1600 rpm in O_2-saturated 0.1 M KOH electrolyte with a scan rate of 10 mVs^{-1}. (c) LSV curves of NGA900 at different rotating rates. The inset shows the corresponding Koutecky–Levich plots at different potentials. (d) Tafel plots of NGA900 and Pt/C in the low-current region. Hollowed symbols show *iR*-corrected data. (e) Summary of the kinetic limiting current density (J_k) and electron-transfer number (n) based on the RDE data of various samples (at 0.365 V vs RHE). (f) Electrochemical stability of the catalysts.

two peaks at the binding energies of ~398.6 and 401.1 eV, corresponding to the pyridinic-N (N1), and graphitic-N (N2), respectively.[56,57] The absence of another typical N species, pyrrolic-N, has been reported to be related to the experimental conditions and the precursor.[32] Distinctly, the shape of these two peaks changed significantly depending on the annealing temperature, indicating a tremendous variety of the relative content of N1 and N2. Relative ratios of the N content are displayed in Figure 5b,c. In NG730, N1 (20.9%) is more prevalent than N2 (9.5%). With increase in the annealing temperature, the total N content decreased dramatically. The N1 (N2) content decreased slowly from 4.3% (4.3%) in NGA800 to 4.2% (3.1%) in NGA850, 3.5% (1.9%) in NGA900, and 2.4% (1.5%) in NGA950. Notably, in NGA1000, only N2 (0.9%) could be distinguished, an indication that only graphitic-N is present in this sample. With increase in the annealing temperature, the ratio of graphitic-N/pyridinic-N (N2/N1) increased significantly to the highest value of ~1.84 for NGA900 (see Figure 5b). This result indicates that during the annealing process, the reconstruction of the carbon framework was accompanied by the variation of N species, and the relative content of different N species can be tuned by controlling the annealing temperature, which might greatly influence the electrocatalytic performances of these N-doped graphene materials.

The electrocatalytic activities were evaluated by CV measurements in 0.1 M KOH solution saturated with O_2 or N_2 at a scanning rate of 50 mV s^{-1}. As shown in Figure 6a, Figure S12 and Figure S13, all the annealed samples show no peak in N_2 saturated solution but an obvious reduction peak in O_2-saturated solution. As the annealed temperature increased, the reduction peak became more postive except the NGA950 and NGA1000, indicating that the ORR catalytic activity was improved. Taking NGA900 as a typical sample, the CV for NGA900 showed a nearly rectangular shape, indicating high conductivity with superior capacitive current. Although a featureless CV in the potential range from 0 to 1.2 V vs RHE was observed in a N_2-saturated solution (Figure 6a). In contrast, a well-defined CV peak (E_{peak}) due to O_2 reduction, centered at 0.795 V vs RHE, can be seen in O_2-saturated solution. Next, to further evaluate the electrocatalytic activity, the N-doped graphene synthesized under different reaction conditions and commercial Pt/C in O_2-saturated 0.1 M KOH(aq) were analyzed by LSV using a rotating disk electrode (RDE) (Figure 4b and Figures S12–S14) at 1600 rpm. We can observe from Figure 6b that with increasing annealing temperature, the limiting current density is increased except for NGA950 and NGA1000. Among all N-doped graphene samples, NGA900 has the highest limiting current density of about 4.6 mA cm^{-2} (at 0.365 V vs RHE), which is comparable to commercial Pt/C (4.63 mA cm^{-2}). The above results reveal that catalytic activity is closely dependent on the annealing temperature, or to say relative content of graphitic-N and pyridinic-N (Figure 5b). As compared with the poor ORR performance of NG730 (E_{peak} = 0.555 V vs RHE), with the increase in the annealing temperature, the onset potential and E_{peak} became more positive, and the current density increases significantly, indicating enhanced ORR catalytic activity. Among them, NGA900 provides the best performance toward ORR, and the onset potential is determined to be ca. 0.914 V vs RHE, which is close to ca. 0.944 V vs RHE identified from commercial Pt/C. The NGA900 sample presents a nearly equal ORR activity to Pt/C catalysts in terms of half-wave potential ($E_{1/2}$) (0.828 V vs RHE and 0.85 V vs RHE for NGA900 and Pt/C, respectively). Recently, carbon-based ORR electrocatalysts with low cost, good durability and various structure including porous carbon, carbon nanotube and graphene attract more and more interest due to the improved ORR activity.[25] For example, Parvez et al. synthesized the N-doped graphene with the $E_{1/2}$ of ~0.775 V vs RHE, and found that the incorporation of Fe into N-doped graphene could signicifantly improve the ORR activity.[58] Ye et al. demonstrated the

DOI: 10.1021/acsami.5b03845
ACS Appl. Mater. Interfaces 2015, 7, 19626–19634

nitrogen-doped carbon with an improved $E_{1/2}$ of about 0.80 V vs RHE,[21] obtained by calcination of a mixture of urea and bacterial cellulose. Next, Qu et al. synthesized N-doped graphene by CVD with an $E_{1/2}$ of ~0.6 V vs RHE and pointed out that the role of N-doping in graphene is important to ORR enhancement.[56] Li et al. developed an electrochemical approach to luminescent and electrocatalytically active N-doped graphene quantum dots with an $E_{1/2}$ of ~0.8 V vs RHE.[59] Chen et al. developed N-doped graphene/carbon nanotube nanocomposite by a hydrothermal process with an $E_{1/2}$ of ~0.73 V vs RHE.[60] He et al. developed three-dimensional (3D) hierarchically porous N-doped carbon catalysts, which exhibited excellent catalytic avtivity with an $E_{1/2}$ of about 0.83 V vs HRE.[22] However, the complicated manipulation process still hindered their further application.[22] To the best of our knowledge, such one-pot direct transformation from graphitic C_3N_4 to nitrogen-doped graphene with high ORR activity has not yet been reported until this work, which has good activities comparable to Pt/C for metal-free N-doped carbon-based catalyst with an $E_{1/2}$ of about 0.828 V vs RHE. Importantly, this synthesis strategy provides a chance to investigate the nature of catalytic sites for ORR in a "clean" binary system with only carbon and nitrogen elements, and no other elements were detected via XPS and ICP analysis, revealing the metal-free nature of NGA samples.

Here, it is postulated that enhanced graphitization degree, tuned relative ratio of different N species, and a proper total content of N in NGA900 have mainly contributed to its superior electrocatalytic activity. To gain further insight into the ORR kinetics, the kinetic current density (J_k) was analyzed based on the RDE tests with various rotating speeds (ω) (Figure 6c). By using the Koutecky–Levich (K–L) equation,[61,62] the number of electron transfers (n) per O_2 molecule involved in the ORR can be determined (inset of Figure 6c). The straight and parallel fitted curves suggest a first-order reaction with the dissolved oxygen on NGA900 from 0.57 to 0.72 V vs RHE. From the slopes of the K–L plots in Figure 6c, the n per O_2 molecule in ORR was calculated to be 3.9 for NGA900 (at 0.365 V vs RHE), indicating a one-step four-electron reduction pathway to produce water as the main product, which will benefit the construction of fuel cells with high efficiency. To shed light on the intrinsic advantage of this novel structure, the Tafel plots for ORR on various electrodes derived from Figure 6c and Figures S12 and S13, are shown in Figure 6d and Figure S15. To compare fairly and accurately the catalytic activity of the annealed samples, the polarization measurements and subsequent Tafel analysis for these iR losses were corrected by the use of the series resistance (Rs), which is determined from the electrochemical impedance spectroscopy as shown in Figure S16. The Tafel plots exhibit two distinct linear regions at both the low and high overpotential regions, and the corresponding Tafel slope values are shown in Figure S17. In the low overpotentical region (>0.865 V vs RHE), the samples give a Tafel slope of ~80 mV dec^{-1} (~78 mV dec^{-1} after iR correction), slightly smaller than that of Pt/C catalysts (92 mV dec^{-1}, ~75 mV dec^{-1} after iR correction), confirming that the ORR activity is dominated by the kinetics of the surface reactions in the low overpotential region.[63] In the higher overpotential range (<0.815 V vs RHE), where the reaction speed is controlled by the diffusion limitation, the Tafel slopes exhibited a relatively stable increase to 91 mV dec^{-1} (~83 mV dec^{-1} after iR correction). As compared to the sharp increase in the Tafel slopes in previously reported metal-free samples,[64] this study shows excellent mass-transfer properties. As shown in Figure 6e and Table S1, an increase in n from 3.2 (NG730) to 3.9 (NGA900) was observed. With the increase in the annealing temperature from 800 to 1000 °C, the kinetic current density (J_k, at 0.365 V vs RHE) keeps at a relatively low value except for NGA900 (Figure 6e). A highest current density of ~29.3 mA cm^{-2} was observed for NGA900, which is even superior to that of the commercial Pt/C (23.7 mA cm^{-2}) under the same testing conditions, further indicating the unique properties of NGA900. Considering the potential applications of NGA900 as effective ORR catalysts by replacing the commercial Pt/C, the electrochemical stability was also investigated.

The NGA900 showed a better long-term durability than the commercial Pt/C. As shown in Figure 6f, after 35 000 s of reaction at 0.715 V vs RHE, 86% of the current density toward ORR can be maintained for NGA900, which is much higher than that of the commercial Pt/C catalyst (33%). Owing to the involvement of metal-free direct transformation, different electrocatalytic activities of the as-prepared N-doped graphene for ORR can be attributed exclusively to the total contents of N and relative ratio of various N species. However, with respect to the nature of catalytic sites in the metal-free catalysts for ORR, inconsistencies are still present.[27,33,34,65,66] For instance, Xing et al. reported that presence of pyridinic-N species on the edge of N-doped graphene is very important for ORR.[33] Conversely, some studies have proved the effect of graphitic N for ORR.[61,66] Very recently, He et al. demonstrated that both pyrrolic- and pyridinic-N are less effective ORR catalytic sites in 3D hierarchically porous N-doped carbons.[22] Lai et al. reported that the electrocatalytic activity of the catalyst was strongly dependent on the graphitic N content, which determined the limiting current density, whereas the pyridinic-N content improved the onset potential for ORR, suggesting that both graphitic- and pyridinic-N could help the ORR peformance.[67] However, they also pointed out that the total N content in the graphene-based nonprecious metal catalyst did not play an important role in determining the ORR property. These conflicting results have attracted great interest because of its great importance in the design of advanced metal-free ORR catalysts. Moreover, it is difficult to identify the role of pyridinic-N that bonds to a metal cation by forming coordination complexes, because its catalytic activity will be affected by the controversial role of metallic impurities.[21] By contrast, our study offers one significant advantage that using the metal-free precursor containing only carbon and nitrogen elements to synthesize the N-doped graphene as electrocatalysts, which may enable us to obtain further insight on the catalytic nature of N-doped carbons for ORR. To get more insight into the ORR performance, the electrical conductivity was first measured by electrochemical impedance spectroscopy (EIS), as shown in Figure S16. It is well accepted that a high electrical conductivity is a prime requirement for ORR catalysts.[22,32] Obviously, the NGA samples exhibited improved electrical conductivity than NG730. NGA900 showed better electrical conductivity than NGA850 and NGA 800, partly explaining its high ORR catalytic activity. Compared to NGA950, better ORR performance with less electrical conductivity observed in NGA900 also implies that the electrical conductivity is not the determining factor for the nature of catalytic sites. As a proof, pure carbon was subjected to the ORR tests under the same experimental conditions, and no obvious ORR electrocatalytic activity was observed. In our

DOI: 10.1021/acsami.5b03845
ACS Appl. Mater. Interfaces 2015, 7, 19626–19634

work, the onset potential and limiting current are improved as the annealing temperature increased except for NGA1000, which means that only appropriate amount of graphitic and pyridinic-N is beneficial for the ORR. On the basis of the XPS analysis, the NGA900 sample shows the highest ratio of graphitic-N/pyridinic-N at a relatively low total N content. It is reasonable to conclude that the increase in electrocatalytic activity can be attributed to the increased ratio of graphitic-N/pyridinic-N as well as a proper total N content.

4. CONCLUSIONS

We have demonstrated a simple and cost-effective approach for the synthesis of N-doped graphene via a direct transformation process. Our synthesis strategy offers a chance to investigate the nature of catalytic sites for ORR in a "clean" binary system, with only carbon and nitrogen elements. The electrochemical tests in combination with XPS analysis proved that the high electrocatalytic activity could be attributed to the improved graphitization degree, high ratio of graphitic-N/pyridinic-N, and proper total content of N. This study may help to elucidate the nature of catalytic sites in metal-free N-doped carbon materials, which is very important for catalyst design and property modulation. Superior ORR performance with good durability rendered the as-prepared N-doped graphene a promising candidate to replace the commercial Pt/C for practical applications.

■ ASSOCIATED CONTENT

Supporting Information

The Supporting Information is available free of charge on the ACS Publications website at DOI: 10.1021/acsami.5b03845.

Experimental section, schematic illustration of the synthesis of N-doped graphene from g-C_3N_4, optical images of the semi-closed quartz tube consisted of C_3N_4 before and after heated at 730° C and optical images of the g-C_3N_4 (0.1 g) heated at different temperature, Raman spectra of NG730 and g-C_3N_4 using a 633 nm laser as the excitation source, total DOS of atom C5, N14, and N16 for $C_{12}N_{16}$, comparison of total energy for $C_{12}N_{16}$ and $C_{21}N_2$, SEM images of g-C_3N_4, heated at 700, 710, and 720 °C, TEM images of the sample heated at different temperatures, nitrogen adsorption/desorption isotherms of NG730 and the corresponding pore size distribution, CV curves of NG730, LSV curves of NG730 and 20% Pt/C from 1V vs RHE to 1.2V vs RHE at 1600 rpm, SEM images of the NG730 and samples annealed at different temperatures, FT-IR spectrum of the annealed samples, high resolution XPS scans of C1s spectra of the NG and NGA samples, CV curves of NGA800 and NGA850, LSV of NGA800 and NGA850 at different rotating speeds, CV curves of NCA950 and NCA1000, LSV of NC950 and NCA1000 at different rotating speeds, Koutechky–Levich plots, Tafel slope the NGA samples, EIS spectra of NG and NGA samples in O_2-saturated KOH solution, Tafel slope values of the NGA samples and commercial Pt/C after *iR* correction, corresponding *n* and J_k obtained from the K–L plots (PDF).

■ AUTHOR INFORMATION

Corresponding Authors

*L. Gu. E-mail: l.gu@iphy.ac.cn.

*P. Xu. E-mail: pxu@hit.edu.cn.

*B. Song. E-mail: songbo@hit.edu.cn. Tel: (+86) 451-86403753. Fax: (+86) 451-86403753.

Notes

The authors declare no competing financial interest.

■ ACKNOWLEDGMENTS

This work was supported financially by the National Natural Science Foundation of China (Grant Nos. 50902037, 51172055, 51372056,51472064, 21471039, 10904024), Science Fund for Creative Research Groups of the National Natural Science Foundation of China (Grant No. 10821201), Fundamental Research Funds for the Central University (Grant Nos. HIT.BRETIII.201220, HIT.NSRIF.2012045, HIT.ICRST.2010008, PIRS of HIT A201502), the Foundation of National Key Laboratory of Science and Technology on Advanced Composite in Special Environment in HIT, International Science & Technology Cooperation Program of China (2012DFR50020) and the Program for New Century Excellent Talents in University (NCET-13-0174). We also thank the High Performance Computing Center of HIT for calculation resource.

■ REFERENCES

(1) Liang, Y.; Li, Y.; Wang, H.; Zhou, J.; Wang, J.; Regier, T.; Dai, H. Co_3O_4 Nanocrystals on Graphene as a Synergistic Catalyst for Oxygen Reduction Reaction. *Nat. Mater.* **2011**, *10*, 780–786.

(2) Debe, M. K. Electrocatalyst Approaches and Challenges for Automotive Fuel Cells. *Nature* **2012**, *486*, 43–51.

(3) Borup, R.; Meyers, J.; Pivovar, B.; Kim, Y. S.; Mukundan, R.; Garland, N.; Myers, D.; Wilson, M.; Garzon, F.; Wood, D.; Zelenay, P.; More, K.; Stroh, K.; Zawodzinski, T.; Boncella, J.; McGrath, J. E.; Inaba, M.; Miyatake, K.; Hori, M.; Ota, K.; Ogumi, Z.; Miyata, S.; Nishikata, A.; Siroma, Z.; Uchimoto, Y.; Yasuda, K.; Kimijima, K.-i.; Iwashita, N. Scientific Aspects of Polymer Electrolyte Fuel Cell Durability and Degradation. *Chem. Rev.* **2007**, *107*, 3904–3951.

(4) Meier, J. C.; Katsounaros, I.; Galeano, C.; Bongard, H. J.; Topalov, A. A.; Kostka, A.; Karschin, A.; Schuth, F.; Mayrhofer, K. J. J. Stability Investigations of Electrocatalysts on the Nanoscale. *Energy Environ. Sci.* **2012**, *5*, 9319–9330.

(5) Steele, B. C. H.; Heinzel, A. Materials for Fuel-Cell Technologies. *Nature* **2001**, *414*, 345–352.

(6) Sasaki, K.; Naohara, H.; Choi, Y.; Cai, Y.; Chen, W.-F.; Liu, P.; Adzic, R. R. Highly Stable Pt Monolayer on PdAu Nanoparticle Electrocatalysts for the Oxygen Reduction Reaction. *Nat. Commun.* **2012**, *3*, 1115.

(7) GreeleyJ; Stephens, I. E. L.; Bondarenko, A. S.; Johansson, T. P.; Hansen, H. A.; Jaramillo, T. F.; Rossmeisl, J.; Chorkendorff, I.; Nørskov, J. K. Alloys of Platinum and Early Transition Metals as Oxygen Reduction Electrocatalysts. *Nat. Chem.* **2009**, *1*, 552–556.

(8) Stamenkovic, V. R.; Fowler, B.; Mun, B. S.; Wang, G.; Ross, P. N.; Lucas, C. A.; Marković, N. M. Improved Oxygen Reduction Activity on $Pt_3Ni(111)$ via Increased Surface Site Availability. *Science* **2007**, *315*, 493–497.

(9) Lefèvre, M.; Proietti, E.; Jaouen, F.; Dodelet, J.-P. Iron-Based Catalysts with Improved Oxygen Reduction Activity in Polymer Electrolyte Fuel Cells. *Science* **2009**, *324*, 71–74.

(10) Liang, Y.; Wang, H.; Zhou, J.; Li, Y.; Wang, J.; Regier, T.; Dai, H. Covalent Hybrid of Spinel Manganese–Cobalt Oxide and Graphene as Advanced Oxygen Reduction Electrocatalysts. *J. Am. Chem. Soc.* **2012**, *134*, 3517–3523.

(11) Liang, Y.; Wang, H.; Diao, P.; Chang, W.; Hong, G.; Li, Y.; Gong, M.; Xie, L.; Zhou, J.; Wang, J.; Regier, T. Z.; Wei, F.; Dai, H. Oxygen Reduction Electrocatalyst Based on Strongly Coupled Cobalt Oxide Nanocrystals and Carbon Nanotubes. *J. Am. Chem. Soc.* **2012**, *134*, 15849–15857.

DOI: 10.1021/acsami.5b03845
ACS Appl. Mater. Interfaces 2015, 7, 19626–19634

(12) Gong, K.; Du, F.; Xia, Z.; Durstock, M.; Dai, L. Nitrogen-Doped Carbon Nanotube Arrays with High Electrocatalytic Activity for Oxygen Reduction. *Science* **2009**, *323*, 760−764.
(13) Zhai, Y.; Dou, Y.; Zhao, D.; Fulvio, P. F.; Mayes, R. T.; Dai, S. Carbon Materials for Chemical Capacitive Energy Storage. *Adv. Mater.* **2011**, *23*, 4828−4850.
(14) Liang, H.-W.; Zhuang, X.; Brüller, S.; Feng, X.; Müllen, K. Hierarchically Porous Carbons with Optimized Nitrogen Doping as Highly Active Electrocatalysts for Oxygen Reduction. *Nat. Commun.* **2014**, *5*, 4973.
(15) Liang, H.-W.; Wei, W.; Wu, Z.-S.; Feng, X.; Müllen, K. Mesoporous Metal−Nitrogen-Doped Carbon Electrocatalysts for Highly Efficient Oxygen Reduction Reaction. *J. Am. Chem. Soc.* **2013**, *135*, 16002−16005.
(16) Wei, W.; Liang, H.; Parvez, K.; Zhuang, X.; Feng, X.; Müllen, K. Nitrogen-Doped Carbon Nanosheets with Size-Defined Mesopores as Highly Efficient Metal-Free Catalyst for the Oxygen Reduction Reaction. *Angew. Chem., Int. Ed.* **2014**, *53*, 1570−1574.
(17) Ma, Z.; Dou, S.; Shen, A.; Tao, L.; Dai, L.; Wang, S. Sulfur-Doped Graphene Derived from Cycled Lithium−Sulfur Batteries as a Metal-Free Electrocatalyst for the Oxygen Reduction Reaction. *Angew. Chem., Int. Ed.* **2015**, *54*, 1888−1892.
(18) Li, Y.; Zhou, W.; Wang, H.; Xie, L.; Liang, Y.; Wei, F.; Idrobo, J.-C.; Pennycook, S. J.; Dai, H. An Oxygen Reduction Electrocatalyst Based on Carbon Nanotube-Graphene Complexes. *Nat. Nanotechnol.* **2012**, *7*, 394−400.
(19) Zhang, Q.; Uchaker, E.; Candelaria, S. L.; Cao, G. Nanomaterials for Energy Conversion and Storage. *Chem. Soc. Rev.* **2013**, *42*, 3127−3171.
(20) Zheng, Y.; Jiao, Y.; Chen, J.; Liu, J.; Liang, J.; Du, A.; Zhang, W.; Zhu, Z.; Smith, S. C.; Jaroniec, M.; Lu, G. Q.; Qiao, S. Z. Nanoporous Graphitic-C_3N_4@Carbon Metal-Free Electrocatalysts for Highly Efficient Oxygen Reduction. *J. Am. Chem. Soc.* **2011**, *133*, 20116−20119.
(21) Ye, T.-N.; Lv, L.-B.; Li, X.-H.; Xu, M.; Chen, J.-S. Strongly Veined Carbon Nanoleaves as a Highly Efficient Metal-Free Electrocatalyst. *Angew. Chem., Int. Ed.* **2014**, *53*, 6905−6909.
(22) He, W.; Jiang, C.; Wang, J.; Lu, L. High-Rate Oxygen Electroreduction over Graphitic-N Species Exposed on 3D Hierarchically Porous Nitrogen-Doped Carbons. *Angew. Chem., Int. Ed.* **2014**, *53*, 9503−9507.
(23) Meng, Y.; Voiry, D.; Goswami, A.; Zou, X.; Huang, X.; Chhowalla, M.; Liu, Z.; Asefa, T. N-, O-, and S-Tridoped Nanoporous Carbons as Selective Catalysts for Oxygen Reduction and Alcohol Oxidation Reactions. *J. Am. Chem. Soc.* **2014**, *136*, 13554−13557.
(24) Mai, L.-Q.; Minhas-Khan, A.; Tian, X.; Hercule, K. M.; Zhao, Y.-L.; Lin, X.; Xu, X. Synergistic Interaction between Redox-Active Electrolyte and Binder-Free Functionalized Carbon for Ultrahigh Supercapacitor Performance. *Nat. Commun.* **2013**, *4*, 2923.
(25) Faber, M. S.; Jin, S. Earth-Abundant Inorganic Electrocatalysts and Their Nanostructures for Energy Conversion Applications. *Energy Environ. Sci.* **2014**, *7*, 3519−3542.
(26) Wang, S.; Iyyamperumal, E.; Roy, A.; Xue, Y.; Yu, D.; Dai, L. Vertically Aligned BCN Nanotubes as Efficient Metal-Free Electrocatalysts for the Oxygen Reduction Reaction: A Synergetic Effect by Co-Doping with Boron and Nitrogen. *Angew. Chem., Int. Ed.* **2011**, *50*, 11756−11760.
(27) Li, Y.; Zhao, Y.; Cheng, H.; Hu, Y.; Shi, G.; Dai, L.; Qu, L. Nitrogen-Doped Graphene Quantum Dots with Oxygen-Rich Functional Groups. *J. Am. Chem. Soc.* **2012**, *134*, 15−18.
(28) Park, H. W.; Lee, D. U.; Zamani, P.; Seo, M. H.; Nazar, L. F.; Chen, Z. Electrospun Porous Nanorod Perovskite Oxide/Nitrogen-Doped Graphene Composite as a Bi-functional Catalyst for Metal Air Batteries. *Nano Energy* **2014**, *10*, 192−200.
(29) Unni, S. M.; Illathvalappil, R.; Gangadharan, P. K.; Bhange, S. N.; Kurungot, S. Layer-Separated Distribution of Nitrogen Doped Graphene by Wrapping on Carbon Nitride Tetrapods for Enhanced Oxygen Reduction Reactions in Acidic Medium. *Chem. Commun.* **2014**, *50*, 13769−13772.
(30) Higgins, D. C.; Hoque, M. A.; Hassan, F.; Choi, J.-Y.; Kim, B.; Chen, Z. Oxygen Reduction on Graphene−Carbon Nanotube Composites Doped Sequentially with Nitrogen and Sulfur. *ACS Catal.* **2014**, *4*, 2734−2740.
(31) Zhang, Y.; Fugane, K.; Mori, T.; Niu, L.; Ye, J. Wet Chemical Synthesis of Nitrogen-Doped Graphene Towards Oxygen Reduction Electrocatalysts without High-Temperature Pyrolysis. *J. Mater. Chem.* **2012**, *22*, 6575−6580.
(32) Wang, D.-W.; Su, D. Heterogeneous Nanocarbon Materials for Oxygen Reduction Reaction. *Energy Environ. Sci.* **2014**, *7*, 576−591.
(33) Xing, T.; Zheng, Y.; Li, L. H.; Cowie, B. C. C.; Gunzelmann, D.; Qiao, S. Z.; Huang, S.; Chen, Y. Observation of Active Sites for Oxygen Reduction Reaction on Nitrogen-Doped Multilayer Graphene. *ACS Nano* **2014**, *8*, 6856−6862.
(34) Geng, D.; Chen, Y.; Chen, Y.; Li, Y.; Li, R.; Sun, X.; Ye, S.; Knights, S. High Oxygen-Reduction Activity and Durability of Nitrogen-Doped Graphene. *Energy Environ. Sci.* **2011**, *4*, 760−764.
(35) Lin, Z.; Waller, G.; Liu, Y.; Liu, M.; Wong, C.-P. Facile Synthesis of Nitrogen-Doped Graphene via Pyrolysis of Graphene Oxide and Urea, and its Electrocatalytic Activity toward the Oxygen-Reduction Reaction. *Adv. Energy Mater.* **2012**, *2*, 884−888.
(36) Zhang, P.; Sun, F.; Xiang, Z.; Shen, Z.; Yun, J.; Cao, D. ZIF-Derived in Situ Nitrogen-Doped Porous Carbons as Efficient Metal-Free Electrocatalysts for Oxygen Reduction Reaction. *Energy Environ. Sci.* **2014**, *7*, 442−450.
(37) Chen, P.; Wang, L.-K.; Wang, G.; Gao, M.-R.; Ge, J.; Yuan, W.-J.; Shen, Y.-H.; Xie, A.-J.; Yu, S.-H. Nitrogen-Doped Nanoporous Carbon Nanosheets Derived from Plant Biomass: An Efficient Catalyst for Oxygen Reduction Reaction. *Energy Environ. Sci.* **2014**, *7*, 4095−4103.
(38) Li, Q.; Xu, P.; Gao, W.; Ma, S.; Zhang, G.; Cao, R.; Cho, J.; Wang, H.-L.; Wu, G. Graphene/Graphene-Tube Nanocomposites Templated from Cage-Containing Metal-Organic Frameworks for Oxygen Reduction in Li−O_2 Batteries. *Adv. Mater.* **2014**, *26*, 1378−1386.
(39) Algara-Siller, G.; Severin, N.; Chong, S. Y.; Björkman, T.; Palgrave, R. G.; Laybourn, A.; Antonietti, M.; Khimyak, Y. Z.; Krasheninnikov, A. V.; Rabe, J. P.; Kaiser, U.; Cooper, A. I.; Thomas, A.; Bojdys, M. J. Triazine-Based Graphitic Carbon Nitride: a Two-Dimensional Semiconductor. *Angew. Chem., Int. Ed.* **2014**, *53*, 7450−7455.
(40) Ma, T. Y.; Dai, S.; Jaroniec, M.; Qiao, S. Z. Graphitic Carbon Nitride Nanosheet−Carbon Nanotube Three-Dimensional Porous Composites as High-Performance Oxygen Evolution Electrocatalysts. *Angew. Chem., Int. Ed.* **2014**, *53*, 7281−7285.
(41) Zheng, Y.; Lin, L.; Ye, X.; Guo, F.; Wang, X. Helical Graphitic Carbon Nitrides with Photocatalytic and Optical Activities. *Angew. Chem., Int. Ed.* **2014**, *53*, 11926−11930.
(42) Wang, X.; Maeda, K.; Thomas, A.; Takanabe, K.; Xin, G.; Carlsson, J. M.; Domen, K.; Antonietti, M. A Metal-Free Polymeric Photocatalyst for Hydrogen Production from Water under Visible Light. *Nat. Mater.* **2009**, *8*, 76−80.
(43) Liu, J.; Liu, Y.; Liu, N.; Han, Y.; Zhang, X.; Huang, H.; Lifshitz, Y.; Lee, S.-T.; Zhong, J.; Kang, Z. Metal-Free Efficient Photocatalyst for Stable Visible Water Splitting Via a Two-Electron Pathway. *Science* **2015**, *347*, 970−974.
(44) Li, Y.; Wang, J.; Yang, Y.; Zhang, Y.; He, D.; An, Q.; Cao, G. Seed-Induced Growing Various TiO_2 Nanostructures on g-C_3N_4 Nanosheets with Much Enhanced Photocatalytic Activity under Visible Light. *J. Hazard. Mater.* **2015**, *292*, 79−89.
(45) Zhang, X.; Xie, X.; Wang, H.; Zhang, J.; Pan, B.; Xie, Y. Enhanced Photoresponsive Ultrathin Graphitic-Phase C_3N_4 Nanosheets for Bioimaging. *J. Am. Chem. Soc.* **2013**, *135*, 18−21.
(46) Zhang, X.; Wang, H.; Wang, H.; Zhang, Q.; Xie, J.; Tian, Y.; Wang, J.; Xie, Y. Single-Layered Graphitic-C_3N_4 Quantum Dots for Two-Photon Fluorescence Imaging of Cellular Nucleus. *Adv. Mater.* **2014**, *26*, 4438−4443.

DOI: 10.1021/acsami.5b03845
ACS Appl. Mater. Interfaces 2015, 7, 19626−19634

(47) Li, X.-H.; Kurasch, S.; Kaiser, U.; Antonietti, M. Synthesis of Monolayer-Patched Graphene from Glucose. *Angew. Chem., Int. Ed.* **2012**, *51*, 9689−9692.
(48) Zhao, H.; Lei, M.; Yang, X. a.; Jian, J.; Chen, X. Route to GaN and VN Assisted by Carbothermal Reduction Process. *J. Am. Chem. Soc.* **2005**, *127*, 15722−15723.
(49) Fischer, A.; Antonietti, M.; Thomas, A. Growth Confined by the Nitrogen Source: Synthesis of Pure Metal Nitride Nanoparticles in Mesoporous Graphitic Carbon Nitride. *Adv. Mater.* **2007**, *19*, 264−267.
(50) Xiang, Q.; Yu, J.; Jaroniec, M. Preparation and Enhanced Visible-Light Photocatalytic H_2-Production Activity of Graphene/C_3N_4 Composites. *J. Phys. Chem. C* **2011**, *115*, 7355−7363.
(51) Kudin, K. N.; Ozbas, B.; Schniepp, H. C.; Prud'homme, R. K.; Aksay, I. A.; Car, R. Raman Spectra of Graphite Oxide and Functionalized Graphene Sheets. *Nano Lett.* **2008**, *8*, 36−41.
(52) Dresselhaus, M. S.; Jorio, A.; Hofmann, M.; Dresselhaus, G.; Saito, R. Perspectives on Carbon Nanotubes and Graphene Raman Spectroscopy. *Nano Lett.* **2010**, *10*, 751−758.
(53) Yan, S. C.; Li, Z. S.; Zou, Z. G. Photodegradation Performance of g-C_3N_4 Fabricated by Directly Heating Melamine. *Langmuir* **2009**, *25*, 10397−10401.
(54) Yap, Y. K.; Kida, S.; Aoyama, T.; Mori, Y.; Sasaki, T. Influence of Negative DC Bias Voltage on Structural Transformation of Carbon Nitride at 600 °C. *Appl. Phys. Lett.* **1998**, *73*, 915−917.
(55) Xue, Y.; Wu, B.; Jiang, L.; Guo, Y.; Huang, L.; Chen, J.; Tan, J.; Geng, D.; Luo, B.; Hu, W.; Yu, G.; Liu, Y. Low Temperature Growth of Highly Nitrogen-Doped Single Crystal Graphene Arrays by Chemical Vapor Deposition. *J. Am. Chem. Soc.* **2012**, *134*, 11060−11063.
(56) Qu, L.; Liu, Y.; Baek, J.-B.; Dai, L. Nitrogen-Doped Graphene as Efficient Metal-Free Electrocatalyst for Oxygen Reduction in Fuel Cells. *ACS Nano* **2010**, *4*, 1321−1326.
(57) Li, X.; Wang, H.; Robinson, J. T.; Sanchez, H.; Diankov, G.; Dai, H. Simultaneous Nitrogen Doping and Reduction of Graphene Oxide. *J. Am. Chem. Soc.* **2009**, *131*, 15939−15944.
(58) Parvez, K.; Yang, S.; Hernandez, Y.; Winter, A.; Turchanin, A.; Feng, X.; Müllen, K. Nitrogen-Doped Graphene and Its Iron-Based Composite As Efficient Electrocatalysts for Oxygen Reduction Reaction. *ACS Nano* **2012**, *6*, 9541−9550.
(59) Li, Y.; Zhao, Y.; Cheng, H.; Hu, Y.; Shi, G.; Dai, L.; Qu, L. Nitrogen-Doped Graphene Quantum Dots with Oxygen-Rich Functional Groups. *J. Am. Chem. Soc.* **2012**, *134*, 15−18.
(60) Chen, P.; Xiao, T.-Y.; Qian, Y.-H.; Li, S.-S.; Yu, S.-H. A Nitrogen-Doped Graphene/Carbon Nanotube Nanocomposite with Synergistically Enhanced Electrochemical Activity. *Adv. Mater.* **2013**, *25*, 3192−3196.
(61) Liu, R.; Wu, D.; Feng, X.; Müllen, K. Nitrogen-Doped Ordered Mesoporous Graphitic Arrays with High Electrocatalytic Activity for Oxygen Reduction. *Angew. Chem., Int. Ed.* **2010**, *49*, 2565−2569.
(62) Chen, W.; Chen, S. Oxygen Electroreduction Catalyzed by Gold Nanoclusters: Strong Core Size Effects. *Angew. Chem., Int. Ed.* **2009**, *48*, 4386−4389.
(63) de Groot, M. T.; Merkx, M.; Wonders, A. H.; Koper, M. T. M. Electrochemical Reduction of NO by Hemin Adsorbed at Pyrolitic Graphite. *J. Am. Chem. Soc.* **2005**, *127*, 7579−7586.
(64) Liang, J.; Zheng, Y.; Chen, J.; Liu, J.; Hulicova-Jurcakova, D.; Jaroniec, M.; Qiao, S. Z. Facile Oxygen Reduction on a Three-Dimensionally Ordered Macroporous Graphitic C_3N_4/Carbon Composite Electrocatalyst. *Angew. Chem., Int. Ed.* **2012**, *51*, 3892−3896.
(65) Li, H.; Kang, W.; Wang, L.; Yue, Q.; Xu, S.; Wang, H.; Liu, J. Synthesis of Three-Dimensional Flowerlike Nitrogen-Doped Carbons by a Copyrolysis Route and the Effect of Nitrogen Species on the Electrocatalytic Activity in Oxygen Reduction Reaction. *Carbon* **2013**, *54*, 249−257.
(66) Niwa, H.; Horiba, K.; Harada, Y.; Oshima, M.; Ikeda, T.; Terakura, K.; Ozaki, J.-i.; Miyata, S. X-Ray Absorption Analysis of Nitrogen Contribution to Oxygen Reduction Reaction in Carbon Alloy Cathode Catalysts for Polymer Electrolyte Fuel Cells. *J. Power Sources* **2009**, *187*, 93−97.
(67) Lai, L.; Potts, J. R.; Zhan, D.; Wang, L.; Poh, C. K.; Tang, C.; Gong, H.; Shen, Z.; Lin, J.; Ruoff, R. S. Exploration of the Active Center Structure of Nitrogen-Doped Graphene-Based Catalysts for Oxygen Reduction Reaction. *Energy Environ. Sci.* **2012**, *5*, 7936−7942.

DOI: 10.1021/acsami.5b03845
ACS Appl. Mater. Interfaces 2015, 7, 19626−19634